J. Fluid Mech. (1980), *vol.* 101, *part* 3, *pp.* 609–629
Printed in Great Britain

The primary electroviscous effect in a suspension of spheres

By J. D. SHERWOOD

Department of Applied Mathematics and Theoretical Physics,
Silver Street, Cambridge

(Received 13 June 1979 and in revised form 25 April 1980)

Previous studies of the distortion of the electric double layer around a charged sphere have assumed that the electric stresses are small compared with the viscous stresses. The flow around the particle is therefore changed only slightly by the presence of the charge cloud. This change is measured by the Hartmann number, and in § 6 we remove the restriction that it should be small. It is found that the previous linearized theory is sufficiently accurate for typical experimental values of the Hartmann number. Previous studies have also assumed that the potential at the surface of the particle is small. This assumption is removed in § 7 of this paper. For values of the non-dimensional surface potential smaller than 2 the predictions are altered by less than 10 %. For higher values the differences between linear and nonlinear theory are not negligible, especially when the charge cloud is thin compared with the radius of the charged sphere.

1. Introduction

The dynamical behaviour of a suspension of charged particles differs from that of a similar but uncharged system. Three mechanisms for these effects have been proposed by Dobry (1953). The 'secondary' effects are caused by interactions between charged particles, while 'tertiary' effects are present when electrical forces cause the particles to change their shape, as happens with polyelectrolytes. Here we shall be concerned with the 'primary' effect. When charged particles are suspended in an electrolyte they attract a cloud of counter-ions. Motion of the fluid distorts the charge cloud producing additional stresses and modifying the Einstein coefficient which characterizes the viscosity in the dilute limit. Previous theories (Booth 1950; Russel 1978; Lever 1979) have assumed that the flow field around the particles is modified only slightly by the presence of the charge cloud. In § 6 we shall remove this restriction.

Booth made the further assumption that the electrical energies of the ions were much smaller than their thermal energies, i.e. $e\psi_0 \ll kT$ where e is the electronic charge, ψ_0 the potential at the surface of the particle, and kT the Boltzmann temperature. This implies that the number density of ions in the charge clouds differs only by $O(e\psi_0/kT)$ from its value in the bulk solution. In nature values of $e\psi_0/kT$ as high as five typically occur, so the second aim of this paper is to remove Booth's assumption that the potential is small. This will be achieved in § 7.

We shall not be concerned with the origin and behaviour of the surface charge. Thus we shall think of any layer of adsorbed ions as being part of the particle itself. The particles will be sufficiently small for the flow to satisfy the Stokes equations, and we

† Present address: Unilever Research Laboratory, Port Sunlight, Wirral, Merseyside.

0022-1120/80/4597-2700 $02.00 © 1980 Cambridge University Press

assume a constant viscosity μ_0 right up to the particle surface. Our surface potential ψ_0 is conventionally known as the ζ-potential.

2. The equilibrium charge cloud

The equations governing the distortion of the charge cloud have been set down by Booth (1950). We assume that the suspending electrolyte contains several species of ions, each with number density n^m and valence z^m. The charge carried by each ion is ez^m and the total charge density ρ is

$$\rho = \sum_m n^m z^m e.$$

Far from any charged particle the number densities of the ions attain limiting values n_∞^m, where

$$\sum_m n_\infty^m z^m e = 0$$

for electrical neutrality of the solution. The electric potential ϕ is given by Poisson's equation:

$$\nabla^2 \phi = -\rho/\epsilon,$$

where we require $\phi = \psi_0$ on the particle surface and $\phi \to 0$ far from the particles. The ions move with the fluid under the influence of electrical and thermodynamic forces. The velocity of an ion of the mth species is therefore

$$\mathbf{v}^m = \mathbf{u} + \omega^m(-ez^m \nabla\phi - kT\nabla \log n^m) \tag{1}$$

where $\mathbf{u}$ is the fluid velocity and ω^m the mobility of the mth species of ion. In future we shall assume that all the ion mobilities are the same, and equal to ω. This approximation is fair for ions of similar molecular size, and enables us to study the charge density rather than the motion of the individual ion species. We shall assume that the ions are not taking part in reactions, and consequently that they satisfy the conservation equation:

$$\frac{\partial n^m}{\partial t} + \nabla . (n^m \mathbf{v}^m) = 0.$$

When $\mathbf{u} = 0$ the charge cloud is in thermal equilibrium and is not distorted by motion of the fluid. Denoting thermal equilibrium by means of the subscript 0, the number density n_0^m of the mth species of ion will be given by the Boltzmann distribution:

$$n_0^m = n_\infty^m \exp[-(ez^m\phi_0/kT)].$$

Inserting this into Poisson's equation gives the Poisson–Boltzmann equation:

$$\nabla^2\phi_0 = -\frac{e}{\epsilon}\sum_m z^m n_\infty^m \exp[-(ez^m\phi_0/kT)].$$

When $e\psi_0 \ll kT$ the exponentials may be expanded as a power series. After linearizing with respect to the small potential, the Poisson–Boltzmann equation becomes

$$\nabla^2\phi_0 = \kappa^2\phi_0$$

where

$$\kappa^2 = \frac{e^2}{\epsilon kT}\sum_m (z^m)^2 n_\infty^m.$$

The Debye length κ^{-1} is a typical size of the charge cloud. We shall not for the moment perform this linearization, but will instead restrict ourselves to an electrolyte containing one species of positive monovalent ions and one of monovalent negative ions, denoted in future by the superscripts + and − respectively.

In one dimension the Poisson–Boltzmann equation may be solved analytically. Setting $p = e\phi_0/kT$ and letting t be the distance from the charged plane, non-dimensionalized with respect to κ^{-1}, the equation becomes:

$$\nabla^2 p = \sinh p.$$

This has solution

$$p = 2\log\left\{\frac{A + e^{-t}}{A - e^{-t}}\right\} \tag{2}$$

where A is a constant of integration which depends on the boundary condition at the plane $t = 0$. In particular, for a plane at a given non-dimensional potential ψ_0

$$A = \frac{e^{\frac{1}{2}\psi_0} + 1}{e^{\frac{1}{2}\psi_0} - 1}.$$

Substituting this into (2), we find when ψ_0 is large that, outside a boundary layer of thickness $e^{-\frac{1}{2}\psi_0}$,

$$p = 2\log\left\{\frac{1 + e^{-t}}{1 - e^{-t}} + O(e^{-\frac{1}{2}\psi_0})\right\}$$

$$\sim 4\left\{e^{-t} + \frac{e^{-3t}}{3} + \ldots + O(e^{-\frac{1}{2}\psi_0})\right\} \quad \text{when} \quad e^{-t} \ll 1.$$

Thus outside the boundary layer the potential saturates and attains a value independent of ψ_0. The far field form is $4e^{-t}$, which is the linearized solution for a plane at potential $\psi_0 = 4$. The presence of a boundary layer of thickness $e^{-\frac{1}{2}\psi_0}$ in which p falls from ψ_0 to a value of order 4 explains the difficulty which is always encountered when solving the Poisson–Boltzmann equation numerically.

We now study the spherically symmetric charge cloud around a sphere of radius a. Non-dimensionalizing the radial distance r from the origin by a, the Poisson–Boltzmann equation becomes

$$\frac{d^2p}{dr^2} + \frac{2}{r}\frac{dp}{dr} = (a\kappa)^2 \sinh p$$

where

$$p = \psi_0 \quad \text{at} \quad r = 1,$$
$$p \to 0 \quad \text{as} \quad r \to \infty.$$

This has to be solved numerically, and the solution is always smaller than the corresponding linearized solution $\phi_0 = \psi_0 e^{a\kappa(1-r)}/r$. However, since the forces on the ions depend on ∇p rather than p, it is not clear whether the electroviscous effect is increased or diminished by linearization. We shall see later that both types of behaviour are possible. A saturation of the equilibrium potential also occurs in three dimensions. Figure 1 shows the coefficient of $e^{a\kappa(1-r)}/r$ in the far field as a function of ψ_0, for various $a\kappa$. As $\psi_0 \to \infty$ each curve attains the limit $\psi_{1\mathrm{lm}}(a\kappa)$. We can see that as $a\kappa \to 0$ the linearized solution is good up to higher potentials, and that for $\psi_0 < 2$ it is accurate to within 10 % whatever the value of $a\kappa$. The variation of $\psi_{1\mathrm{lm}}$ with $a\kappa$ is shown in figure 2.

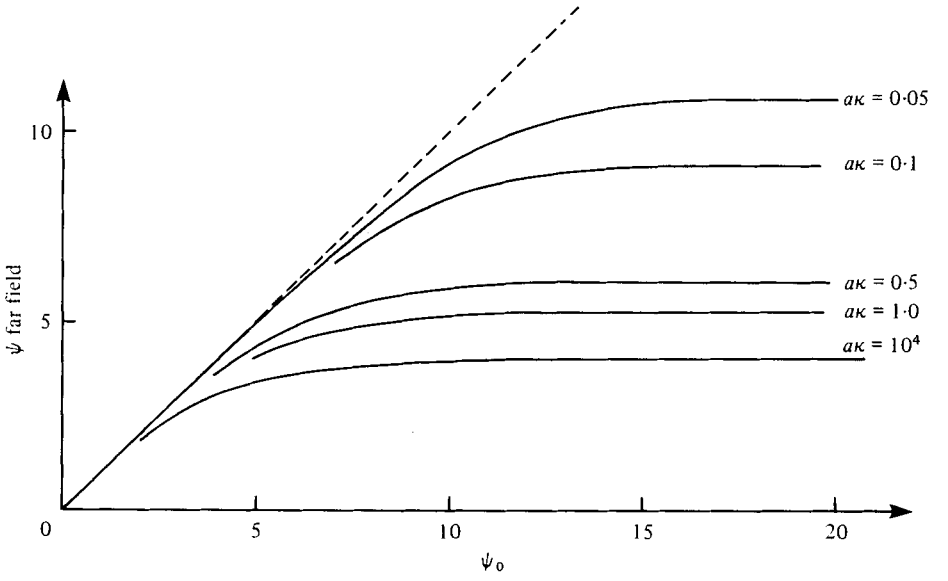

FIGURE 1. The coefficient of $e^{a\kappa(1-r)}/r$ in the far field of an equilibrium spherical charge cloud, for various $a\kappa$.

When $a\kappa \gg 1$ curvature is negligible. We may attempt a series solution of the Poisson–Boltzmann equation, expanding p as $p_0+p_1+\ldots$ where p_i is $O(a\kappa)^{-i}$. Defining an inner variable t by $r = 1+t/a\kappa$, we find that p_0 is simply the plane potential (2), while

$$p_1 = \frac{2A\,e^{-t}}{a\kappa(A^2-e^{-2t})}\left(\frac{1-e^{-2t}}{A^2}-2t\right).$$

Taking the limit $\psi_0 \to \infty$ (i.e. $A \to 1$) we find

$$p_0+p_1 \to e^{-t}\left(4+\frac{2}{a\kappa}\right)-\frac{4te^{-t}}{a\kappa} \quad \text{as} \quad t\to\infty.$$

This inner expansion is valid only for $t \lesssim a\kappa$, but when $a\kappa$ is large the potential decays sufficiently in the inner region for the linearized solution to be valid in the outer region, and matching implies

$$\psi_{\text{llm}} \sim 4+\frac{2}{a\kappa}, \quad a\kappa \gg 1.$$

When $a\kappa \ll 1$ the term $(a\kappa)^2\sinh(p)$ in the Poisson–Boltzmann equation will not be as large as $\nabla^2 p$ near the particle unless $p \sim -\log(a\kappa)$. Errors caused by linearization of $\sinh(p)$ will therefore not be significant at smaller potentials, and from figure 2 we see

$$\psi_{\text{llm}} \sim 3-2{\cdot}6\log(a\kappa) \quad \text{as} \quad a\kappa \to 0. \tag{3}$$

Close to a highly charged surface the Poisson–Boltzmann equation predicts an exponentially large number density of counter-ions. Since each ion has finite size, such a high density might not be attainable. Moreover, we have neglected such effects as discreteness of the charge, ion–ion interactions, ion–surface interactions and variations in the dielectric constant of the solvent close to the particle surface. Levine &

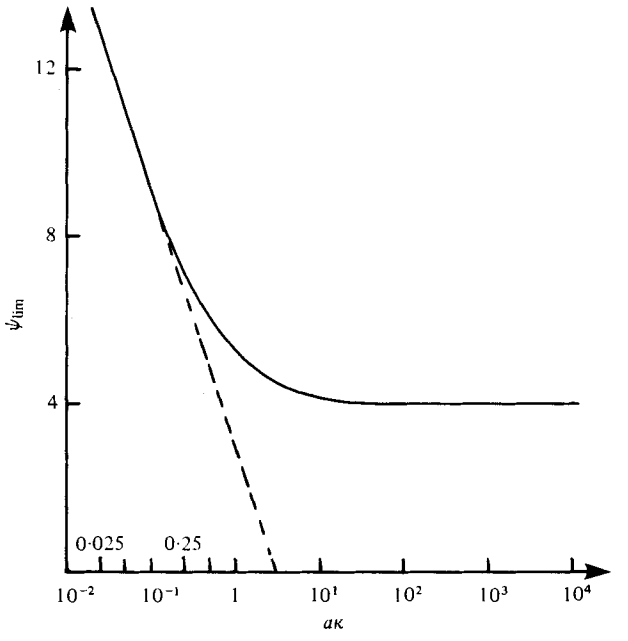

FIGURE 2. $\psi_{\lim}$ = coefficient of $e^{a\kappa(1-r)}/r$ in a saturated equilibrium charge cloud, as a function of $a\kappa$.

Bell (1966) have estimated that for $\psi_0 \leqslant 3$, with an ion concentration $\leqslant 0{\cdot}1$ moles/litre, the corrections may be neglected, since they tend to cancel each other. Despite all the attention lavished upon the equilibrium double layer, no generally valid theory has been produced. In order to render our electroviscous problem tractable, there seems no alternative but to adopt the unmodified Poisson–Boltzmann equation.

3. The distortion of the charge cloud and of the fluid motion around each particle

Weak potentials

We first examine the distortion of the charge cloud caused by motion of the fluid. Let us assume that $e\psi_0 \ll kT$: this implies that the electrical energy of the ions is small compared with their thermal energy. The ion concentration n^m therefore differs only by $O(e\psi_0/kT)$ from its value n_∞^m far from any particle. Substituting the expression (1) for the ion velocity $\mathbf{v}$ into the ion conservation equation, we may then neglect terms which are $O(e\psi_0/kT)^2$. This enables us to perform a summation over the ion species to obtain

$$\nabla^2\rho - \kappa^2\rho = \nabla . (\mathbf{u}\rho)/\omega kT. \tag{4}$$

Equation (4) represents a balance between the convective forces deforming the charge cloud, and the electric and thermal forces tending to restore equilibrium. The ratio of these two effects is measured by the Péclet number $Pe = U/\omega kT\kappa$, where U is a typical velocity. For a shear flow of strength Γ with a typical length scale κ^{-1}, Pe becomes $\Gamma/\omega kT\kappa^2$. We assume Pe to be small, which is valid if Γ is typically much smaller than 10^8 s^{-1}. Russel (1978) and Lever (1979) have removed this restriction

but only in the limits of very thin and very thick charge clouds, respectively. Expanding ρ as $\rho_0+\rho_1+\ldots$, where ρ_i is $O(Pe)^i$, (with a similar expansion for ϕ), we obtain first from (4) and from Poisson's equation the equilibrium charge cloud $\phi_0 = -\rho_0/\epsilon\kappa^2$, where for a spherical particle of radius a,

$$\rho_0 = -\epsilon\kappa^2\psi_0 a\, e^{\kappa(a-r)}/r.$$

The first corrections ρ_1 and ϕ_1 caused by the weak flow are governed by

$$\nabla^2\rho_1 - \kappa^2\rho_1 = \nabla\cdot(\mathbf{u}\rho_0)/\omega kT \tag{5}$$

and

$$\nabla^2\phi_1 = -\rho_1/\epsilon. \tag{6}$$

We assume that the suspending fluid has viscosity μ_0, is incompressible, and that its motion is governed by the Stokes equation:

$$0 = \mu_0\nabla^2 u - \nabla p - \rho\nabla\phi$$

where the last term is the electrostatic body force. Expanding it for weak flow we find that at the lowest order the unperturbed term $\rho_0\nabla\phi_0$ may be absorbed into the pressure and has no dynamical significance. The $O(Pe)$ correction is governed by

$$\mu_0\nabla^2\mathbf{u} = \nabla p + \rho_0\nabla(\phi_1+\rho_1/\epsilon\kappa^2)$$

after again absorbing a term into the pressure. Since ρ_1 is typically $O(U\epsilon\kappa\psi_0/\omega kT)$ and ρ_0 is typically $O(\epsilon\kappa^2\psi_0)$ the presence of the charge cloud causes a change $\mathbf{u}'$ in the velocity, where $|\mathbf{u}'|/U \sim \psi_0^2\epsilon/\omega kT\mu_0$. This non-dimensional group, known as the electric Hartmann number He, measures the ratio of the electric and viscous forces acting on the fluid. However, in the case of a thin charge cloud (i.e. $a\kappa \gg 1$), only the velocity component normal to the surface distorts the charge cloud. Since this component varies only quadratically with distance from the surface, the distortion of the cloud is $O(Pe/a\kappa)$ and hence

$$H_e = \begin{cases} \psi_0^2\epsilon/\omega kT\mu_0 a\kappa & \text{for } a\kappa \gg 1, \\ \psi_0^2\epsilon/\omega kT\mu_0 & \text{otherwise.} \end{cases}$$

The quantity $\phi_1+\rho_1/\epsilon\kappa^2 = \chi$ say, appears in the Stokes equation and will recur throughout the analysis. It was used by Booth (1950), but with little explanation. We may think of $\nabla\chi$ as the force acting on the charge cloud. $\rho\nabla\phi_1$ is the perturbed electric force acting on the ions, while $\nabla\rho_1$ is proportional to the thermodynamic force. Hence $\nabla\chi$ is the net force restoring equilibrium. Combining (5) and (6) gives an equation governing χ alone:

$$\nabla^2\chi = \mathbf{u}\cdot\nabla\rho_0/\omega kT\kappa^2\epsilon, \tag{7}$$

where we have used the incompressibility of the fluid. Our boundary condition is that there should be no flux of ions into the surface of the particle, and hence $\mathbf{j}\cdot\mathbf{n} = 0$ there, where $\mathbf{n}$ is normal to the surface and $\mathbf{j}$ is the current density. We are therefore neglecting any flow of ions into or out of the Stern layer of adsorbed ions. Little is known about the non-equilibrium behaviour of the Stern layer, but if its capacity is small, or relaxation time large, then any surface currents will be small. By an appropriate summation of (1) over all ion species, we find

$$\mathbf{j} = \rho_0\mathbf{u} - \omega kT\epsilon\kappa^2\nabla\chi.$$

Hence $\mathbf{n}.\nabla\chi = 0$ on the surface of the particle, since $\mathbf{u}.\mathbf{n} = 0$ there. At infinity the charge cloud and any perturbation decay to zero.

The distorted charge cloud with arbitrary surface potentials

We now remove the restriction that $e\psi_0 \ll kT$, though instead, as in § 2, we restrict ourselves to one species of positive monovalent ions and one of monovalent negative ions. We again assume that the Péclet number is small, and we therefore expand the ion densities n as $n_0 + n_1$, where n_1 is $O(Pe)$. We expand ϕ similarly. Linearizing in the small Péclet number, the ion velocities may be written as

$$\mathbf{v}^{\pm} = \mathbf{u} - \frac{\omega kT}{n_\infty}\nabla\chi_{\pm},$$

where

$$\chi_{\pm} = n_1^{\pm} e^{\pm p} \pm \phi_1 e n_\infty / kT.$$

The ion conservation equation is now

$$\nabla.(n^{\pm}\mathbf{v}^{\pm}) = 0.$$

To leading order in the Péclet number this is

$$\nabla^2\chi_+ - \nabla p.\nabla\chi_+ = -\frac{n_\infty}{\omega kT}\mathbf{u}.\nabla p, \tag{8a}$$

$$\nabla^2\chi_- + \nabla p.\nabla\chi_- = +\frac{n_\infty}{\omega kT}\mathbf{u}.\nabla p. \tag{8b}$$

The boundary condition that there should be no flux of ions into the surface requires $\mathbf{n}.\nabla\chi_{\pm} = 0$. We again require that the charge cloud and its perturbation decay at infinity: i.e. $\chi_{\pm} \to 0$ as $r \to \infty$.

4. The stress

We follow the presentation due to Batchelor (1970), as modified to include electrical effects by Russel (1976). The contributions of the particles and their double layers to the stress was shown by Russel to be

$$\frac{1}{V}\sum_{\text{particles}}\oint_{S_n}\mathbf{x}\,\boldsymbol{\sigma}.\mathbf{n} - \mu_0(\mathbf{un} + \mathbf{nu})\,dA + \frac{1}{V}\int_{V-\Sigma V_n}\rho\mathbf{x}\nabla\phi\,dV, \tag{9}$$

where S_n, V_n are the surface and volume of the nth particle in the volume V. We now assume that the suspension is dilute: the particles therefore contribute separately to the stress. If there were no electrical effects the surface integral would give Einstein's term for the increase in the stress. However, the electrical force $-\rho\nabla\phi$ alters the flow of the fluid and thereby modifies this surface integral. Rather than compute this alteration to the entire flow field, we may instead immediately obtain the surface integral via the reciprocal theorem. This makes use of a second, comparison, problem in which there are no body forces and in which the particle is assumed to deform with a given straining rate. If the velocity **U** outside a rigid particle in a straining flow

$\mathbf{E}.\mathbf{x}$ is written in the form $\mathbf{U} = \mathbf{F}.\mathbf{E}$, where $\mathbf{F}$ is a third-rank tensor constant, then the reciprocal theorem shows that the total electrical contribution to the stress is

$$\int_{V_f} \rho \nabla\phi . \mathbf{F} dV, \tag{10}$$

where the integral is over all space outside the particle.

For weak potentials we can again make our small Péclet number expansion of ρ and ϕ. Using the properties of $\mathbf{F}$, (10) may be expanded, correct to the first order in the Péclet number, in the forms

$$\int_{V_f} \nabla\chi . \mathbf{F}\rho_0 dV = -\int_{V_f} \nabla\rho_0 . \mathbf{F}\chi dV. \tag{11}$$

Thus we see that, when $Pe \ll 1$, χ is indeed the only perturbed quantity required.

For arbitrary potentials the stress (10) may be put into the form

$$\int_{V_f} \nabla\phi_0 . \mathbf{F} e\{e^{-p}\chi_+ - e^{p}\chi_-\}. \tag{12}$$

Thus the contributions of the two types of ion to the stress integral (12) are uncoupled, as are the equations (8) governing the perturbations of the ionic charge cloud. We may now compare our theories for weak and for arbitrary potentials. $\nabla\chi$ gives the total force on the charge cloud, while $\nabla\chi_\pm$ give the forces on the individual ion species. When ψ_0 is small, $\chi_\pm$ become $n_1^\mp \pm n_\infty e\phi_1/kT$ implying that $e\chi_+ - e\chi_- = \epsilon\kappa^2\chi$. Thus $\chi_+ - \chi_-$ is $O(\psi_0)$ as $\psi_0 \to 0$. Adding equations (8*a*) and (8*b*) we obtain

$$\nabla^2(\chi_+ + \chi_-) = \nabla p . \nabla(\chi_+ - \chi_-).$$

Hence $\chi_+ + \chi_-$ is $O(\psi_0^2)$ as $\psi_0 \to 0$ and does not enter the linearized theory. We may pursue this line of analysis further in order to obtain results for small potentials as an expansion in ψ_0. This problem is tractable when $a\kappa \gg 1$ yielding a contribution to the viscosity

$$\frac{15\epsilon}{(a\kappa)^2\omega kT}\left(\frac{kT}{e}\right)^2 \Phi\left\{\psi_0^2 + \frac{\psi_0^4}{64} - \frac{\psi_0^6}{3\cdot 2^{10}} + \ldots\right\} \quad \text{as} \quad \psi_0 \to 0. \tag{13}$$

Here Φ is the volume fraction of particles in the suspension, and ψ_0 is non-dimensionalized with respect to kT/e. For small ψ_0 the effect is larger than predicted by linear theory, while there is a suggestion that for larger potentials there could be a maximum. However, (13) is maximal at $\psi_0 = 7{\cdot}2$, which is well outside the range of validity of the expansion.

5. Restriction to spherical particles

Weak potentials

The expression (10) for the stress applies to rigid particles of arbitrary shape. We now restrict our attention to a spherical particle of radius a. Suppose the flow imposed at infinity is linear and equal to $\mathbf{E}.\mathbf{x} + \boldsymbol{\Omega}.\mathbf{x}$ where $\mathbf{E}$ is the symmetric strain-rate tensor and $\boldsymbol{\Omega}$ the antisymmetric vorticity tensor. The flow around the sphere in the absence of electrical effects is

$$\boldsymbol{\Omega}.\mathbf{x} + \left(1 - \frac{a^5}{r^5}\right)\mathbf{E}.\mathbf{x} + \mathbf{x}\frac{\mathbf{x}.\mathbf{E}.\mathbf{x}}{r^2}\cdot\frac{5}{2}\left(\frac{a^5}{r^5} - \frac{a^3}{r^3}\right). \tag{14}$$

As Russel (1978) explains, the vorticity merely rotates the particle and its charge cloud without distorting the cloud, so to the first order in the weak flow it has no effect. The governing equations form a sixth-order set of differential equations which fortunately are separable by spherical harmonics, so we look for solutions of the form

$$\chi = \frac{\mathbf{x}.\mathbf{E}.\mathbf{x}}{r^2} q(r) \frac{\psi_0 a^2}{\omega k T},$$

$$\mathbf{u} = \mathbf{E}.\mathbf{x} g(r) + \mathbf{x} \frac{\mathbf{x}.\mathbf{E}.\mathbf{x}}{r^2} f(r).$$

The functions f and g for an uncharged particle are given in (14), which also shows that $\mathbf{F} = \mathbf{Ix}(1-a^5r^{-5}) - 5\mathbf{xxx}(a^3r^{-3} - a^5r^{-5})/2$. We now scale lengths by the radius of the sphere. This is done for convenience in the numerical computation and results in the parameter $a\kappa$ appearing explicitly in some analytic expressions. For example, the Hartmann number becomes $M = 2\epsilon\psi_0^2(a\kappa)^2/\omega k T \mu_0$ where the factor 2 is introduced for convenience. The Stokes equation, and those representing the distortion of the charge cloud (7) and the incompressibility of the fluid become

$$f''' + 9f''r^{-1} + 6f'r^{-2} - 30fr^{-3} = M(a\kappa r^{-3} + r^{-4})\, e^{a\kappa(1-r)} q(r), \tag{15}$$

$$q'' + 2q'r^{-1} - 6qr^{-2} = -e^{a\kappa(1-r)}(g+f)(a\kappa + r^{-1}), \tag{16}$$

$$g' + f' + 3fr^{-1} = 0, \tag{17}$$

with boundary conditions

$$f, q, (g-1) \to 0 \quad \text{at} \quad \text{infinity},$$
$$q', f, g = 0 \quad \text{at} \quad r = 1.$$

Having found χ, we must finally evaluate the stress integral (11). Performing the angular integrations analytically, we find that the electrical contribution to the viscosity in a suspension of volume fraction Φ is $2\Phi\psi_0^2\epsilon(a\kappa)^2 J/\omega k T = MJ\Phi$ where

$$J = \int_1^\infty q(r)\, e^{a\kappa(1-r)}(2r + 3r^{-4} - 5r^{-2})(1 + a\kappa r)\, dr/20.$$

Arbitrary potentials

In the more general case we know the potential $p(r)$ only as a numerical solution of the Poisson–Boltzmann equation, and we inevitably must solve the equations (8) for $\chi_\pm$ numerically. We look for solutions of the form

$$\begin{Bmatrix} \chi_+ \\ \chi_- \end{Bmatrix} = \frac{n_\infty a^2}{\omega k T} \frac{\mathbf{x}.\mathbf{E}.\mathbf{x}}{r^2} \begin{Bmatrix} q_+(r) \\ q_-(r) \end{Bmatrix},$$

where by (8)

$$q_+'' + 2r^{-1}q_+' - 6r^{-2}q_+ - p'q_+' = -rp'(1 - 2{\cdot}5r^{-3} + 1{\cdot}5r^{-5}), \tag{18a}$$

$$q_-'' + 2r^{-1}q_-' - 6r^{-2}q_- + p'q_-' = +rp'(1 - 2{\cdot}5r^{-3} + 1{\cdot}5r^{-5}), \tag{18b}$$

with boundary conditions

$$q_\pm' = 0 \quad \text{at} \quad r = 1,$$
$$q_\pm \sim O(r^{-3}) \quad \text{as} \quad r \to \infty.$$

In equation (18) we have used the velocity field appropriate to low Hartmann numbers

as given by equation (14). The angular integrations in the stress integral (12) may be performed to give the increase in the stress of the suspension:

$$\Phi \frac{(a\kappa)^2}{5} \frac{\epsilon}{\omega k T} \left(\frac{kT}{e}\right)^2 \mathbf{E} I,$$

where

$$I = \int_1^\infty (1 - 2{\cdot}5r^{-3} + 1{\cdot}5r^{-5}) (q_+ e^{-p} - q_- e^{p}) \frac{dp}{dr} r^3 \, dr.$$

6. The Hartmann number

Small Hartmann numbers

In this section we shall investigate how strongly our results depend upon the Hartmann number. We therefore postpone our study of arbitrary potentials to § 7: like Booth, we shall assume here that the surface potential is weak. Booth found χ using the unperturbed velocity field (14) in equation (16), and then calculated the change in the stress. This method merely gives the leading term in an expansion for small Hartmann numbers. Higher terms may be obtained by an iterative process. Having found χ we may use this result in the Stokes equations (15) and (17) to give a correction to $\mathbf{u}$. Returning to (16) we obtain a correction to χ, and so the process continues. The problem is tractable in the limit of a thin charge cloud ($a\kappa \gg 1$), and predicts

$$\mu = \mu_0 \left(1 + \tfrac{5}{2}\Phi \left(1 + \frac{6\epsilon\psi_0^2}{\omega k T (a\kappa)^2 \mu_0} \left(1 - \frac{\epsilon\psi_0^2}{\omega k T \mu_0 a\kappa} + \ldots\right)\right)\right).$$

First comes Einstein's $\frac{5}{2}$ term for uncharged spheres and the second term is that obtained by Booth. The final term is $O(H_e^2)$ and we note the appearance of the Hartmann number predicted in § 3.1 for the case $a\kappa \gg 1$. This additional term is negative: the flow is modified so as to reduce the perturbation of the charge cloud (cf. Lenz's law). More generally, numerical solutions of the governing equations (15)–(17) indicate that motion of the fluid diminishes as the electric forces increase, and the electroviscous effect therefore grows more slowly than the linear predictions of Booth's theory. When the Hartmann number becomes very large these solutions show the fluid adjacent to the particle to be almost at rest. We shall first study these high Hartmann numbers analytically and then look in more detail at the numerical results.

High Hartmann numbers

When the Hartmann number is large we intuitively expect the fluid close to the sphere to be held at rest by the strong electric forces which would be created by any perturbation of the charge cloud. These electrical effects decay exponentially away from the sphere, while the viscous stresses vary only algebraically and therefore dominate far from the particle. In between these two extremes there will be a transition region in which the two sets of forces balance. We expect this region to have size κ^{-1}, the length scale on which the charge cloud decays. The numerical results confirm our intuition. We examine each of the three regions in turn.

We approach the problem via the method of matched asymptotic expansions. Near the sphere $e^{a\kappa(1-r)}$ is $O(1)$ and it is impossible to balance the large parameter M against the highest derivatives of f and q in (15) and (16). We must therefore conclude

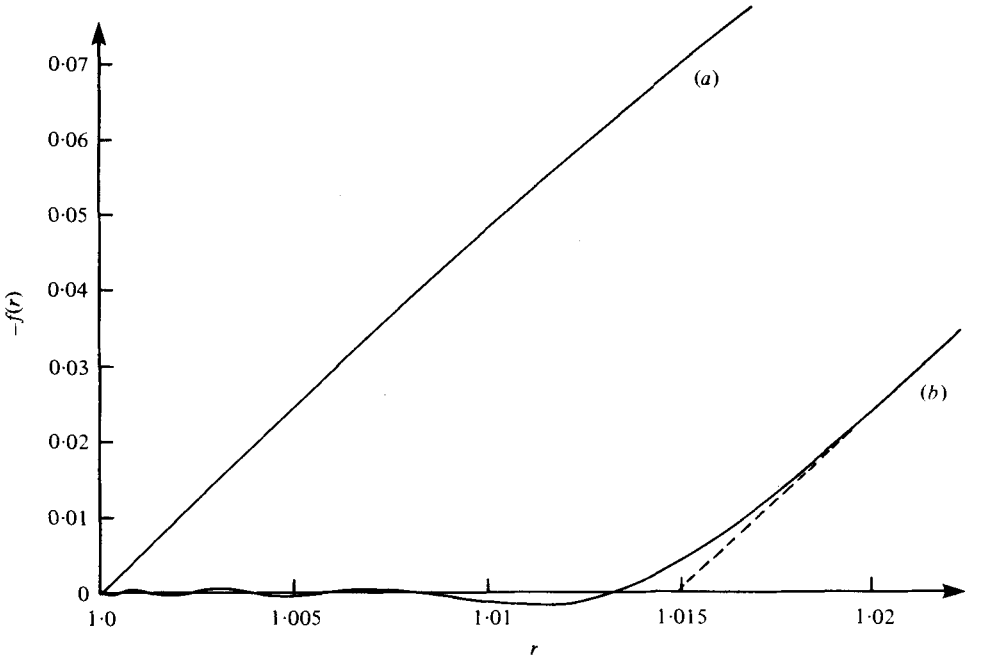

FIGURE 3. The flow function $-f(r)$ plotted against radial position r for $a\kappa = 500$, (*a*) for $M = 0$, (*b*) for $M = 10^{16}$. All but the last oscillation in (*b*) are too small to be shown to scale.

that f and q are each exponentially small when $(r-1)$ is small. Any perturbation to the charge cloud produces restoring forces so strong that the flow and perturbation are reduced almost in zero. A balance becomes possible at $r \sim R$, where

$$e^{a\kappa(1-R)} = (a\kappa R)^2 M^{-\frac{1}{2}}, \tag{19}$$

i.e.

$$R \sim \frac{\ln M}{2a\kappa} \quad \text{as} \quad M \to \infty.$$

This asymptotic estimate is accurate only at very large M, and we shall prefer numerical solutions of equation (19). The asymptotic analysis is thus applicable when aR, the dimensional radius of the sphere in which there is little motion, is much larger than the length scale κ^{-1} over which the electric fields decay.

At distances within $O(a\kappa)$ of $r = R$ the electric forces and viscous forces can balance. To investigate this region we define an inner variable y by $r = R + y/a\kappa$ and expand f as $f_1 + f_2 + \ldots$, where f_i is $O(f_{i-1}/Ra\kappa)$. We expand q and g similarly. The dominant terms of the governing equations (15)–(17) are then

$$\begin{aligned} f_{1yyy} &= M^{\frac{1}{2}} e^{-y} q_1/R, \\ q_{1yy} &= -e^{-y} R^2 a\kappa (g_1 + f_1) M^{-\frac{1}{2}}, \\ g_{1y} + f_{1y} &= -3f_1/Ra\kappa. \end{aligned}$$

We can see clearly the balance between $f_1 \sim M^{\frac{1}{2}} q_1$ and $q_1 \sim (g_1 + f_1) M^{-\frac{1}{2}}$. For $y \gg 1$ solutions have the form

$$f_1 \sim A e^{-y} + B e^{-2y} + C y e^{-y} + D + Ey + Fy^2 \quad \text{as} \quad y \to \infty.$$

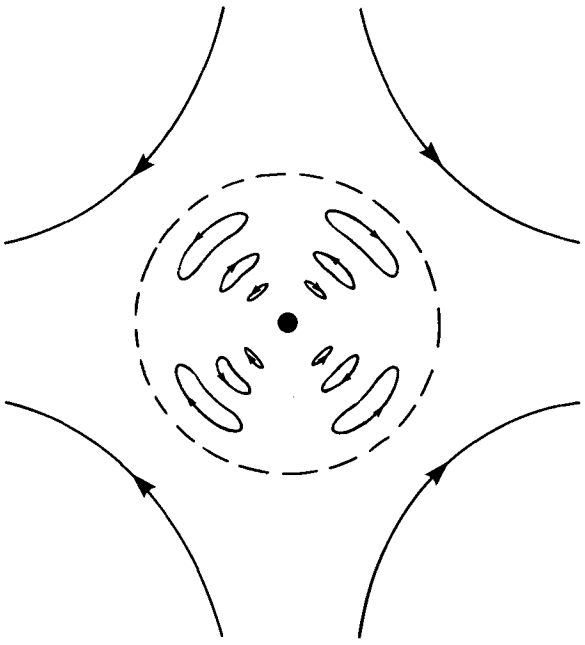

FIGURE 4. Sketch of the eddies which occur at high Hartmann numbers.

For $y \ll -1$ we balance the highest derivatives against the large factor e^{-y} to obtain solutions which decay as $y \to -\infty$:

$$\exp[-3^{\frac{7}{6}}e^{-\frac{1}{3}y}] \quad \text{and} \quad \exp\left[-\frac{3^{\frac{7}{6}}}{2}e^{-\frac{1}{3}y}\right]\begin{matrix}\sin\\ \cos\end{matrix}\left[\frac{3^{\frac{5}{3}}}{2}e^{-\frac{1}{3}y}\right]. \tag{20}$$

Thus we can have solutions which are exponentially small for small r, as required. Since the oscillatory solutions decay the more slowly, we expect them to dominate as $y \to -\infty$. Figure 3 shows $-f$ given by the numerical solution of the full equations at $M = 10^{16}$, $a\kappa = 500$; g and q exhibit similar oscillations. The zeros of (20) occur at $3^{\frac{5}{3}}e^{-\frac{1}{3}y}/2 = n\pi + \theta$ where θ is some unknown phase. As n becomes large the half period for r approaches $(3a\kappa)^{-1}\ln(1+n^{-1})$. The decay between successive maxima is

$$\exp(-3^{\frac{1}{3}}\pi) = (6{\cdot}133)^{-1}.$$

When $a\kappa = 500$ and $M \gg 1$ this period and rate of decay are in good agreement with the full numerical solutions. When $a\kappa = 0{\cdot}5$ oscillations also occur, though the highest value of $Ra\kappa$ studied was only 4·5, and quantitative agreement was poor. We may interpret these oscillations as a series of eddies, depicted in figure 4. Moffatt (1964) found that the magnetic field due to a line current can produce two-dimensional eddies by inhibiting radial motion in magneto-hydrodynamic flows. In our problem it is the electric field which inhibits radial flow.

In the far field we expect a solution which varies on the length scale of the effective radius R. We choose an outer variable $w = Rr$ and look for solutions of the form $f = \alpha w^{-3} + \beta w^{-5}$, $g = 1 - 2\beta/5w^5$, $q = \gamma w^{-3}$. Matching $(f+g)$ with the solution in the transition region we obtain $1 + \alpha + \frac{3}{5}\beta = 8B/Ra\kappa$. Matching q gives $\gamma = -ARM^{-\frac{1}{2}}$, while matching f gives $\alpha + \beta = 0$, to leading order. Hence $\beta = -a = \frac{5}{2}$ + corrections. Thus the far field is flow around a rigid sphere of radius R.

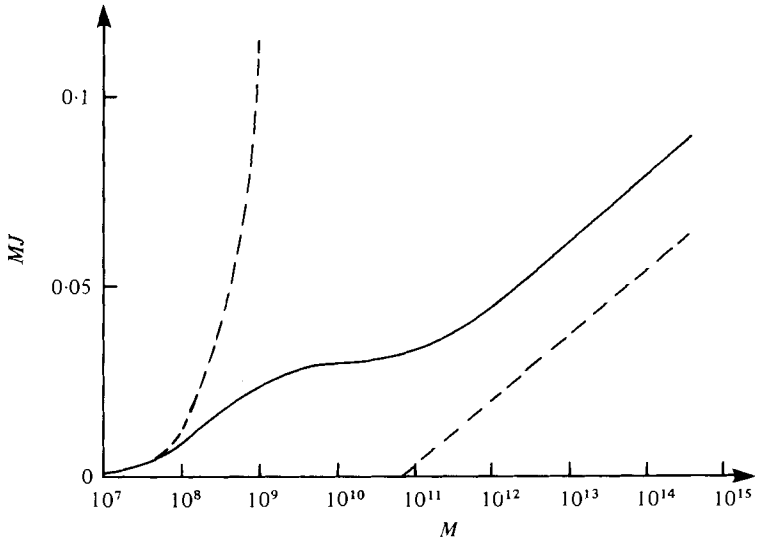

FIGURE 5. The increase MJ in the intrinsic viscosity due to electrical forces, plotted against M, for $a\kappa = 500$. The numerical computations are given by the solid curve and the asymptotic predictions for $M \to 0$ and $M \to \infty$ are given by broken lines.

The particle contribution to the bulk stress can be derived from the stress integral J. Alternatively one can look at Russel's (1976) derivation of expression (9), and note that it may be applied to any surface S_n surrounding the particle. If we choose a surface outside $r = R$ the electrical forces contribute little to the volume integral, while the surface integral yields the result for a rigid sphere of radius R. Thus we find that the viscosity of the suspension becomes

$$\mu_0(1+\tfrac{5}{2}\Phi R^3) \quad \text{as} \quad M \to \infty,$$

where R increases only slowly as M increases.

Numerical results

In general we must solve the governing equations (15)–(17) numerically. They form a sixth-order set of equations, with three boundary conditions at $r = 1$ and three at infinity. A fourth order Runge–Kutta scheme was used, shooting outwards from $r = 1$ to beyond the charge cloud, where the nature of the algebraic decay of f, q and $(g-1)$ is known. Since the equations are linear, four shots suffice to determine the behaviour of the solution for large r as a function of the initial conditions at $r = 1$: a fifth shot then successfully attains the boundary conditions. When $M = 0$ the numerical results agree with Booth's theory, and for $a\kappa \gg 1$, $M \ll 1$ they agree with the results given in § 6.1. The behaviour was found to be similar for all values of $a\kappa$, so two cases, $a\kappa = 0{\cdot}5$ and 500, were investigated in detail and pursued to as high a value of M as possible. When $a\kappa = 0{\cdot}5$ we require $M = 10$ before there is a 3 % decrease in J. When $a\kappa = 500$ and $M = 10^7$, J has decreased by less than 4 %. However, this very large value of M corresponds to the Hartmann number given earlier for thin charge clouds being just 0·04.

In figure 5 we plot the change in the intrinsic viscosity due to electrical forces, MJ,

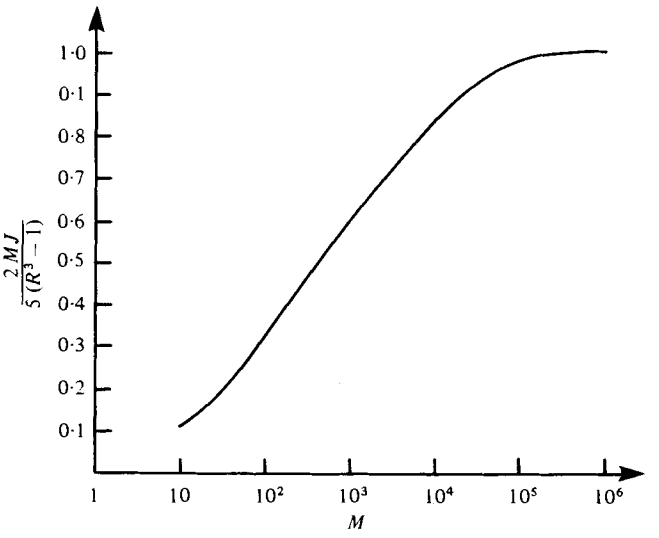

FIGURE 6. The numerical value of MJ divided by the asymptotic prediction at $a\kappa = 0{\cdot}5$.

against M when $a\kappa = 500$. For small M, J is constant and so the intrinsic viscosity is proportional to M. Although J decreases for larger M, we observe that the intrinsic viscosity always increases as M increases. The theoretical prediction $MJ \sim \frac{5}{2}(R^3-1)$ for large M is also plotted, where we have used R as obtained numerically from equation (18). There is a difference of 0·003 between this value of R and the one given by a full solution of the governing equations. The two curves of figure 5 are therefore parallel but not coincident. This difference becomes unimportant as R becomes large; to remove it we should have to pursue further the asymptotic expansion and analysis. Figure 6 shows the ratio of the computed values of MJ to the asymptotic predictions for large M when $a\kappa = 0{\cdot}5$. As $Ra\kappa$ becomes large the numerical result rapidly approaches the asymptotic theory. When $M = 10^6$, $MJ = 1{\cdot}9 \times 10^3$ and is large, but $Ra\kappa$ is still only 4·5.

In conclusion, then, the electrical contribution to the intrinsic viscosity, MJ, is less than predicted by Booth's small-Hartmann-number theory. However, the experimental values of M encountered are not usually very large. In the experiments of Stone-Masui & Watillon (1968) H_e is typically 6, while $a\kappa$ is typically 1. Thus M is typically at most .12 and Booth's theory overestimates the result by 3 %. Although the non-dimensional number H_e measuring the strength of the electrical forces is often not small, as assumed by Booth, we may conclude that in practical conditions it is not sufficiently large to significantly affect his predictions. We shall use this result to simplify the analysis of arbitrary potentials in § 7, where we shall assume that the Hartmann number is small.

7. Arbitrary surface potentials

The numerical scheme

We assumed throughout § 6 that the potential ψ_0 was small. We now remove this assumption. Instead of solving equation (16) to find χ, we must now consider separately the individual ion species, solving (18) to obtain $\chi_\pm$. The motion of the fluid is still governed by the Stokes equation, but the results of § 6 tell us that the flow will not differ greatly from that around an uncharged sphere (14), and this will suffice for our purposes. There is therefore no need to consider an equation, analogous to (15), for the motion of the fluid.

The differential equations were solved using a fourth-order Runge–Kutta scheme. In this case, though, we must first find a numerical solution of the nonlinear Poisson–Boltzmann equation which governs the unperturbed charge cloud. This was solved using a shooting technique, starting at the surface of the particle ($r = 1$). Ideally a freely varying step-length should be used in order to accommodate the thin boundary layer close to the particle. However, since the results were to be tabulated and used to find $\chi_\pm$, it proved convenient to make at most two changes of steplength. The integral I was computed by Simpson's rule. Halving all step lengths suggests that the accuracy was about 1 %, except for the very highest potentials when there may be 5 % errors.

Booth's (1950) theory predicts an electrical contribution to the viscosity which is proportional to ψ_0^2 and the numerical results increase quadratically when ψ_0 is small. In the following sections we study the behaviour when $e\psi_0/kT$ becomes large, and compare our analytic predictions with the numerical results. When $a\kappa \gg 1$ the intrinsic viscosity first increases to a maximum as ψ_0 increases, and then decreases to a limiting value (see figure 8). In § 7.2 we predict the initial increase in the intrinsic viscosity, but the analysis breaks down before the maximum is attained. In § 7.3 we study the region beyond the maximum. When $a\kappa \ll 1$ the intrinsic viscosity increases monotonically to a limiting value as ψ_0 increases (see figure 9) and we study this case in § 7.4.

Thin charge cloud with intermediate potentials $1 \ll e^{\frac{1}{2}\psi_0} \ll a\kappa$

When the double layer is thin we may to a first approximation neglect curvature. Taking $t = a\kappa(r-1)$ as an inner variable, the equilibrium potential is given by the one-dimensional solution (2). In terms of the inner variable the equation for χ_+, (18*a*), becomes

$$q_{+tt} - p_t q_{+t} + \frac{2q_{+t}}{a\kappa} - \frac{6q_+}{(a\kappa)^2} = -\frac{15}{2} p_t \frac{t^2}{(a\kappa)^3}. \tag{21}$$

We may neglect $q_{+t}/a\kappa$ in comparison with $p_t q_{+t}$ near the surface, since $p_t \gg 1$. We assume that q_+ is not sufficiently large for $q_+(a\kappa)^{-2}$ to be important and verify this at the end. Integrating (21) once and matching with an outer solution of the form $C_1 r^{-3}$ outside the charge cloud, we find that $C_1 = -20\log 2(a\kappa)^{-2} = q_+(0)$. Including the term $6q_+(a\kappa)^{-2}$ on the right-hand side of (21) as a correction, we find that it is indeed negligible. Following exactly the same argument for q_-, we obtain

$$q_-(0) = 10(\psi_0 - 2\log 2)(a\kappa)^{-2}$$

but we find that the term $6q_-(a\kappa)^{-2}$ is negligible only if $\psi_0 \ll 2\log(a\kappa)$. When this

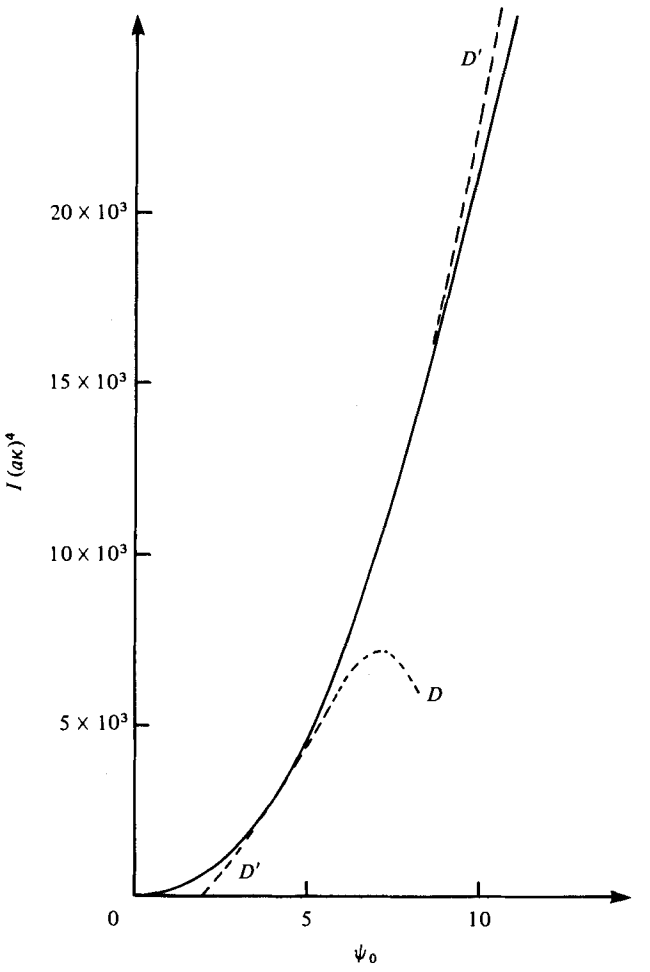

FIGURE 7. The stress integral $I(a\kappa)^4$ as a function of ψ_0 when $a\kappa = 10^4$. The broken line D shows the expansion (13) valid for small potentials, while the broken line D' shows the predictions of §7.2.

holds, both q_+ and q_- vary only slowly in the inner region. The stress integral I can now be evaluated. The positive ions are excluded from the innermost region close to the positively charged particle, and are present only in the outer part of the charge cloud. In the limit $\psi_0 \to \infty$ their contribution to the stress integral becomes

$$1200(\log 2)^2\,(a\kappa)^{-4}$$

which is independent of ψ_0. This reflects the saturation of the outer part of the cloud. The Boltzmann distribution for the number density of the negative ions increases exponentially as we approach the particle, and their contribution

$$\sim 300(\psi_0 - 2\log 2)^2\,(a\kappa)^{-4}$$

as $\psi_0 \to \infty$. Hence

$$I \sim 300(\psi_0^2 - 4\psi_0 \log 2 + 8\log^2 2)\,(a\kappa)^{-4} + O(a\kappa)^{-5}$$

which may be compared with the result $I \sim 150\psi_0^2(a\kappa)^{-4}$ as $\psi_0 \to 0$.

Figure 7 shows the numerical results for $I(a\kappa)^4$ as a function of ψ_0 when $a\kappa = 10^4$. When ψ_0 is small, we may compare them with the expansion (13), which is shown as a broken curve D. The first term alone of (13) is out by 5 % at $\psi_0 = 2$, while all three terms together are accurate to within 5 % at $\psi_0 = 5$. A second broken line D' indicates the asymptotic result of this section. This is accurate to within 5 % when $\psi_0 = 5$. Because the analysis eventually breaks down, the upper limit of acceptable accuracy depends on $a\kappa$, and when $a\kappa = 10^4$ we have 5 % accuracy up to $\psi_0 = 9$.

Thin charge cloud with high potentials $1 \ll (a\kappa)^2 \ll (a\kappa)^2\psi_0 \lesssim e^{\frac{1}{2}\psi_0}$

Figure 8 shows the numerical results for $I(a\kappa)^4$ as a function of ψ_0 for several large values of $a\kappa$. The stress integral I is scaled by $(a\kappa)^4$ so that all curves should coalesce onto the expansion for small potentials (13). We may note, however, that (13), regarded as an expansion in powers of $(a\kappa)^{-1}$ is poor unless $a\kappa \gg 100$, since the next term is

$$\mu = \mu_0 + \tfrac{5}{2}\mu_0\Phi + \frac{15\epsilon}{(a\kappa)^2\omega kT'}\left(\frac{kT}{e}\right)^2 \Phi\psi_0^2\left\{1 - \frac{317}{16a\kappa} + O(a\kappa)^{-2}\right\} \quad \text{as} \quad a\kappa \to \infty.$$

The striking feature of figure 8 is the maximum which occurs on each curve. To the left of the maximum the intermediate theory of § 7.2 holds, though it has hardly any chance to become established unless $a\kappa \geqslant 100$. This analysis, however, breaks down when ψ_0 is no longer small compared with $\log(a\kappa)$. We now study the high potentials to the right of the maximum.

When $\psi_0 \gg 1$ the equilibrium potential p varies rapidly across a region of thickness $t \sim e^{-\frac{1}{2}\psi_0}$. We also know from (18*b*) that the Taylor expansion for q_- is

$$q_- = q_-(0)\,(1 + 3t^2(a\kappa)^{-2} + \ldots)$$

when t is small. The equation for q_- equivalent to (21) is

$$(e^p q_{-t})_t - 6q_- e^p (a\kappa)^{-2} + 2q_{-t} e^p (a\kappa)^{-1} = 15p_t e^t t^2/2(a\kappa)^3.$$

As before, we neglect the third term on the left-hand side, but in § 7.2 we found that the second term is important at very high potentials. We may re-write the equation as

$$\begin{aligned} e^p q_{-t} &= \int_0^t \left\{ p_t e^p \frac{15t^2}{2(a\kappa)^3} + 6q_- \frac{e^p}{(a\kappa)^2} \right\} \\ &= -\frac{30A}{(a\kappa)^3}\left\{ \frac{-t^2 e^{-t}}{(A - e^{-t})^2} - \frac{2te^{-t}}{A(A - e^{-t})} + \frac{2}{A}\log\left(\frac{A - e^{-t}}{A - 1}\right)\right\} \\ &\quad + 6q_-(0)\frac{e^{\frac{1}{2}\psi_0}}{(a\kappa)^2}\left\{2 + e^{-\frac{1}{2}\psi_0}\left(t - \frac{4}{A - e^{-t}}\right)\right\} + O(a\kappa)^{-4} \\ &\sim \frac{-30}{(a\kappa)^3}\left\{ \frac{-t^2 e^{-t}}{(A - e^{-t})^2} - \frac{2te^{-t}}{A - e^{-t}} + 2\log(A - e^{-t}) + \psi_0 - 2\log 2 \right\} \\ &\quad + 12q_-(0)\frac{e^{\frac{1}{2}\psi_0}}{(a\kappa)^2} \quad \text{as} \quad \psi_0 \to \infty \\ &= F(t), \quad \text{say.} \end{aligned}$$

The term $q_-(0)\,e^{\frac{1}{2}\psi_0}$ comes from the integral $\int q_- e^p\,dt$ with $t = O(e^{-\frac{1}{2}\psi_0})$. We should therefore add to $F(t)$ a correction $\int 6\tilde{q}_- e^p (a\kappa)^{-2}\,dt$ where $q_- = q_-(0) + \tilde{q}(t)$. However since $\tilde{q}_-$ is $O(q_-(0)\,e^{-\psi_0})$ when $t = O(e^{-\frac{1}{2}\psi_0})$ there is no large contribution from this correction. If we are to match q_- with an outer solution $c_2 r^{-3}$ valid outside the charge

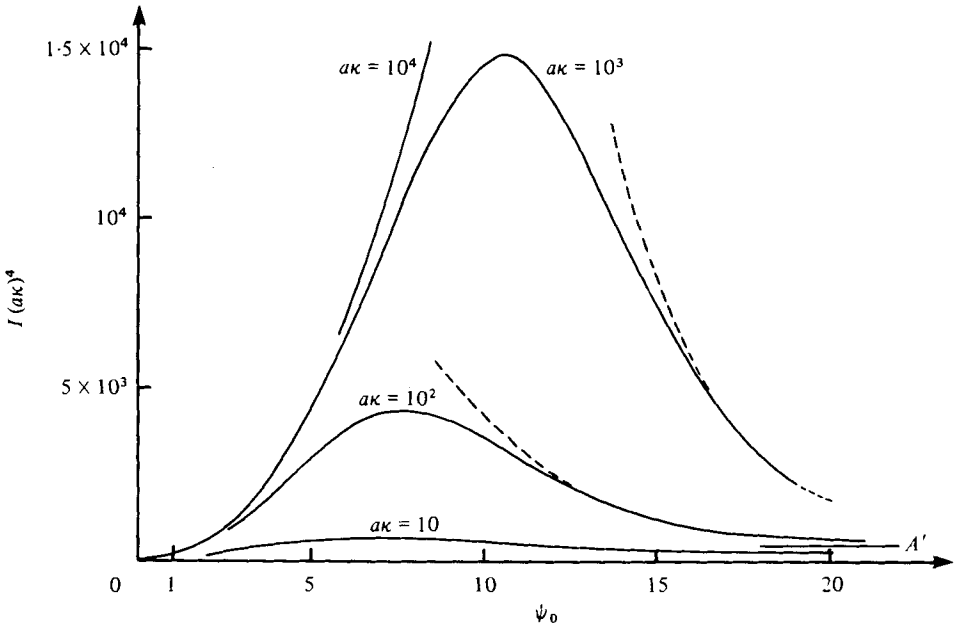

FIGURE 8. The stress integral $I(a\kappa)^4$ as a function of ψ_0 for various large values of $a\kappa$. The broken line indicates the predictions of §7.3. The line A' shows the contribution of the positive ions when $a\kappa = 100$.

cloud, we require q_{-t} to be $O(F/a\kappa)$ for large t, where F is defined above, and hence the two large constants must vanish, i.e.

$$-\frac{30}{(a\kappa)^3}(\psi_0 - 2\log 2) + 12q_-(0)\frac{e^{\frac{1}{2}\psi_0}}{(a\kappa)^2} = 0$$

implying

$$q_-(0) = 5\frac{(\psi_0 - 2\log 2)}{2a\kappa}e^{-\frac{1}{2}\psi_0}.$$

When $a\kappa = 100$ this agrees with the full numerical result to within 1 % for $\psi_0 \geqslant 16$. When matching with the outer solution we assumed that q_- was typically $O(F)$ and hence that $q_-(0)$ was no larger than $|F|$ i.e. $\psi_0 e^{-\frac{1}{2}\psi_0} \lesssim (a\kappa)^{-2}$. This therefore defines the range of validity of the analysis. The dominant contribution of the negative ions to the stress integral I comes once again from the region near $t = 0$, and is

$$75(\psi_0 - 2\log 2)^2 e^{-\frac{1}{2}\psi_0}(a\kappa)^{-3} + O(\psi_0^2 e^{-\frac{1}{2}\psi_0}(a\kappa)^{-4}) + O(a\kappa)^{-5} \quad \text{as} \quad \psi_0 \to \infty$$

(since corrections to p are $O(p(a\kappa)^{-1})$ and corrections to q_- are $O(F(a\kappa)^{-2})$). Hence as $\psi_0 \to \infty$ the contribution of the negative ions decays to $O(a\kappa)^{-5}$, while the positive ions still contribute $O(a\kappa)^{-4}$. The full expression for I is

$$I \sim 75(\psi_0 - 2\log 2)^2 e^{-\frac{1}{2}\psi_0}(a\kappa)^{-3} + 1200(a\kappa)^{-4}\log^2 2 + O(a\kappa)^{-5} \quad \text{as} \quad \psi_0 \to \infty.$$

The positive ions are still repelled from the particle into the outer, saturated, part of the charge cloud. Their behaviour has not changed, and is still given by §7.2, but we must examine the new behaviour of the negative ions. The distortion of the spherical charge cloud is caused by motion of the fluid normal to the surface, near which

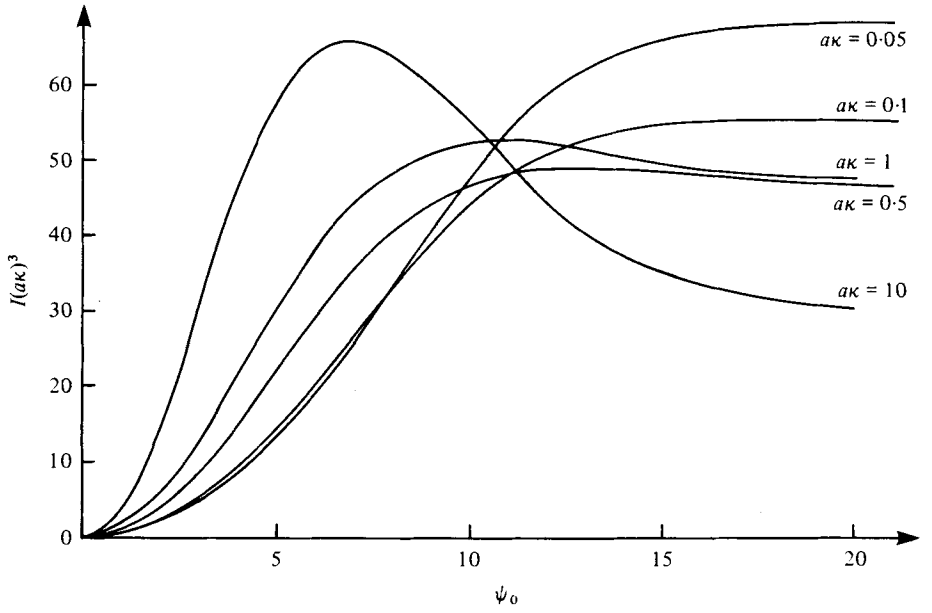

FIGURE 9. The stress integral $I(a\kappa)^3$ as a function of ψ_0 for various thick charge clouds.

$\mathbf{u}.\mathbf{n} \propto t^2$. Hence in the innermost boundary layer of thickness $e^{-\frac{1}{2}\psi_0}$ the normal flux of ions is $O(n_\infty)$. For a given perturbation n_1^- of the charge cloud, $\chi_- \sim n_1^- e^{-p}$ and is small, as is the non-equilibrium force on the ions $\nabla\chi_- \sim n_1^- e^{-p}\nabla p$. However, this force acts on the large number of ions $n_\infty e^p$ in the boundary layer and the resulting flux is $O(n_1^- n_\infty \nabla p)$. A balance between these fluxes in the ion conservation equation is only possible if the perturbation of the charge cloud in the boundary layer is very small i.e. if $q_-(0) \to 0$ as $\psi_0 \to \infty$. Russel found no such restriction when the potential was small, and the resulting large tangential forces on the ions gave the dominant contribution to the stress. These tangential forces have disappeared now that the perturbation of the cloud is small.

The predicted values of the stress I are shown on figure 8 by broken lines. To demonstrate that it is indeed the contribution of the positive ions that dominates at large potentials, the line A' shows their contribution when $a\kappa = 100$, as calculated numerically. It is $4{\cdot}9 \times 10^{-6}$, rather than the $5{\cdot}8 \times 10^{-6}$ predicted in § 7.2.

Thick charge clouds with high potentials

Figure 9 shows the behaviour of $I(a\kappa)^3$ as ψ_0 increases for various small values of $a\kappa$. I is scaled by $(a\kappa)^3$ so that all curves should coalesce onto Booth's results for thick charge clouds when the potential is small. As the charge cloud becomes thicker, the maximum in the curves disappears, and we are left with monotonic increase to a limiting value. We may easily grasp the physical mechanism governing thick charge clouds without resorting to a mathematical analysis. Lever (1979) has shown that at small potentials the dominant contribution to the stress integral comes from the large $O(\kappa^{-3})$ volume of the charge cloud rather than the small $O(a^3)$ volume near the particle, and that the boundary conditions on the surface of a point-particle form an inner

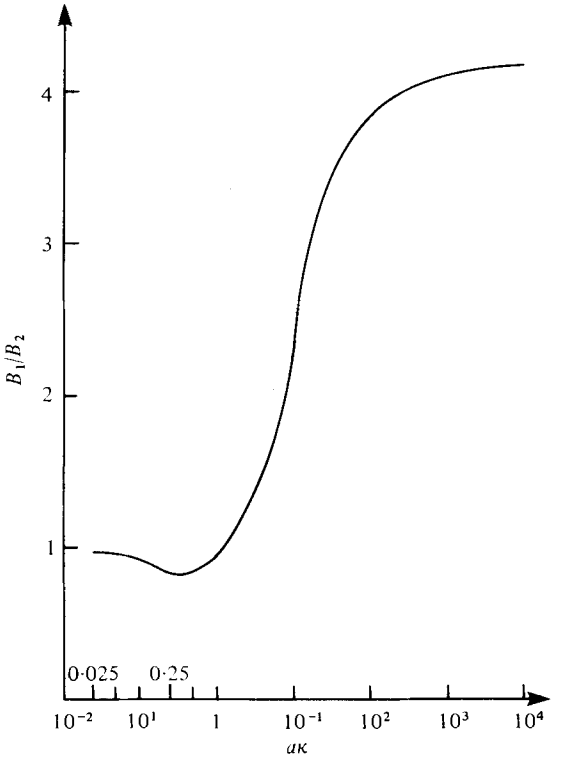

FIGURE 10. B_1/B_2 as defined by equation (22), as a function of $a\kappa$, showing the approach to unity as $a\kappa \to 0$.

problem which may be neglected. Hence the important region is exactly that in which the equilibrium potential saturates. I suggest here that the saturation of the equilibrium charge cloud is the dominant effect, and that the theory for small potentials need only be modified in this one respect. Thus we expect that

$$B_1 = \frac{\lim_{\psi_0 \to \infty} (I)}{\psi_{\lim}^2} \doteq \lim_{\psi_0 \to 0} \left\{ \frac{I}{\psi_0^2} \right\} = B_2, \quad \text{say.} \tag{22}$$

In figure 10 the ratio B_1/B_2 is plotted against $\log(a\kappa)$. It does indeed approach 1 as $a\kappa \to 0$. Booth found that $B_2 \sim 0{\cdot}5(a\kappa)^{-3}$ when $a\kappa \ll 1$. Using the result (3) for $\psi_{\lim}$ as $a\kappa \to 0$ we obtain

$$I \sim \frac{(3 - 2{\cdot}6 \log a\kappa)^2}{2(a\kappa)^3} \quad \text{as} \quad \psi_0 \to \infty \quad \text{when} \quad a\kappa \ll 1.$$

Figure 11 shows the ratio of the numerical results to Booth's predictions for small potentials, i.e. it shows $I/(B_2\psi_0^2)$ as a function of ψ_0. We see that Booth's theory is reasonable up to $\psi_0 = 2$, where the error is less than 10 %. The sign of the error varies. Booth's theory is always an overestimate when $a\kappa$ is small, but when $a\kappa$ is large it is first an under-estimate. When $\psi_0 = 5$ the numerical result is 40 % below Booth's predictions at $a\kappa = 10$, and 20 % above at $a\kappa = 10^3$. We may also see that Booth's theory is accurate up to higher potentials as the charge cloud becomes thicker, because the onset of saturation of the charge cloud is delayed. We have pursued the analysis

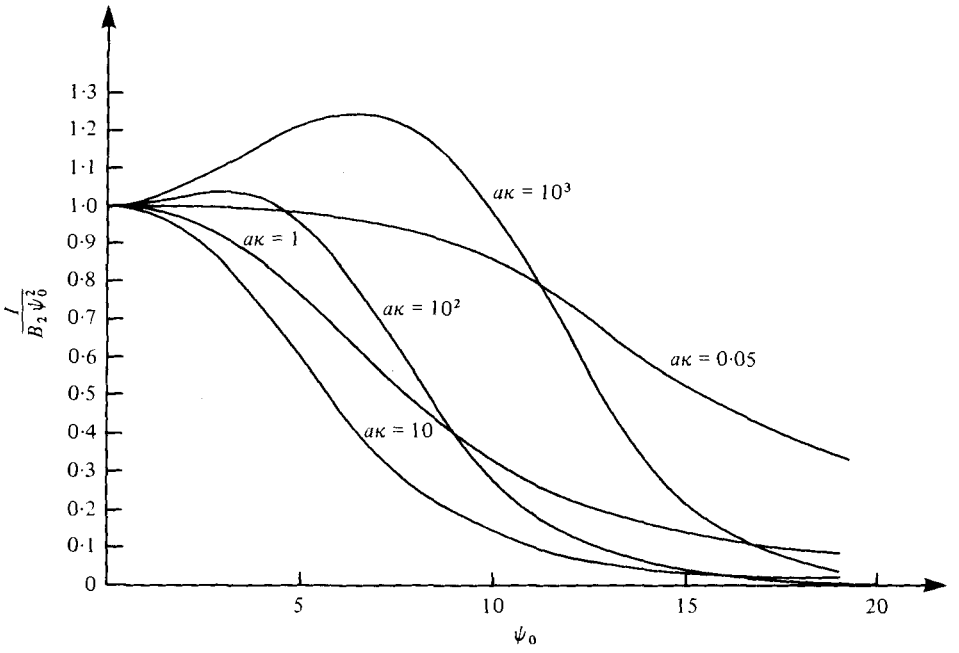

FIGURE 11. The ratio of the full numerical results to Booth's linearized theory.

up to very high potentials in order to understand the physical mechanisms involved. In nature, however, potentials rarely exceed five. Even so, the modification to earlier theories is not negligible and must be included in any interpretation of experimental results.

O'Brien & White (1978) have recently studied electrophoresis. Because this involves motion caused by the application of a uniform electric field, the perturbations to the charge cloud take the form of first harmonics rather than second. Otherwise the problem, and the results they obtained in a numerical study, are similar: they too found maxima occurring when $a\kappa$ was large, and monotonic increase to a limit when $a\kappa$ was small.

The author is grateful to his supervisor, Dr E. J. Hinch, for his advice and encouragement throughout this work, which was supported financially by the Science Research Council.

REFERENCES

BATCHELOR, G. K. 1970 *J. Fluid Mech.* **41**, 545.
BOOTH, F. 1950 *Proc. Roy. Soc.* A **203**, 533.
DOBRY, A. 1953 *J. Chim. Phys.* **50**, 507.
LEVER, D. A. 1979 *J. Fluid Mech.* **92**, 421.
LEVINE, S. & BELL, G. M. 1966 *Discuss. Faraday Soc.* **42**, 69.
MOFFATT, H. K. 1964 *J. Fluid Mech.* **18**, 1.
O'BRIEN, R. W. & WHITE, L. R. 1978 *J.C.S. Faraday II* **74**, 1607.
RUSSEL, W. B. 1976 *J. Colloid Interface Sci.* **55**, 590.
RUSSEL, W. B. 1978 *J. Fluid Mech.* **85**, 209.
STONE-MASUI, J. & WATILLON, A. 1968 *J. Colloid Interface Sci.* **28**, 187.